ment in the output data level is obtainable by using a pin-guide photodiode with possible association to a passive reactive 30–40 GHz matching circuit [7].

ACKNOWLEDGMENT

The authors would like to thank CNET-France Telecom for their financial support, and E. Penard from CNET Lannion and N. Haese from IEMN-DHS for fruitful discussions.

REFERENCES

1. H. Ogawa, D. Polifko, and S. Banba, "Millimeter-Wave Fiber Optics Systems for Personal Radio Communication," *IEEE Trans. Microwave Theory Tech.*, Vol. 40, Dec. 1992, pp. 2285–2293.
2. J. B. Georges, D. M. Cutrer, O. Solgaard, and K. Y. Lau, "Optical Transmission of Narrowband Millimeter-Wave Signals," *IEEE Trans. Microwave Theory Tech.*, Vol. 43, Sept. 1995, pp. 2229–2240.
3. Z. Ahmed, D. Novak, R. B. Waterhouse, and H. F. Liu, "Optically-Fed Millimetre-Wave (37 GHz) Transmission System Incorporating a Hybrid Mode-Locked Semiconductor Laser," *Electron. Lett.*, Vol. 32, Sept. 1996, pp. 1790–1792.
4. F. Devaux, P. Bordes, J. F. Cadiou, E. Penard, J. Guena, and P. Legaud, "Distribution of Millimetre Radiowave Signals with an MQW Electroabsorption Modulator," *Electron. Lett.*, Vol. 30, Sept. 1994, pp. 1522–1524.
5. T. Ido, S. Tanaka, M. Suzuki, M. Koizumi, H. Sano, and H. Inoue, "Ultra-High Speed Multiple-Quantum-Well Electro-Absorption Optical Modulators with Integrated Waveguides," *J. Lightwave Technol.*, Vol. 14, Sept. 1996, pp. 2026–2034.
6. D. Mathoorasing and C. Kazmierski, "Efficient Optical Harmonic Converter with 1.5 μm MQW DFB VUG Laser for Millimeter Wave Radio Applications," *Electron. Lett.*, Vol. 30, Nov. 1994, pp. 1957–1958.
7. J. C. Renaud, "Optoelectronic Devices for Microwave Optical Links," *Proc. European Conf. Networks and Opt. Commun. (NOC'96)*, Heidelberg, Germany, 1996.

© 1997 John Wiley & Sons, Inc.

CCC 0895-2477/97

A HIGHLY ACCURATE GUMMEL PLOT MODEL FOR THERMAL DESIGN OF HIGH-POWER MICROWAVE HBTs

Byoung-Uk Ihn[1] and Bumman Kim[1]
[1]Department of Electrical and Electronic Engineering
and Microwave Application Research Center
Pohang University of Science and Technology
San-31 Hyoja-dong, Nam-Gu, Pohang, Kyungbuk, 790-784, Korea

Received 1 April 1997

ABSTRACT: *An accurate Gummel plot model of HBT at a wide range of current level and temperatures has been established. The model contains a bias- and temperature-dependent parasitic resistance and temperature-dependent temperature coefficient of base–emitter turn-on voltage. The average error between the measurement data and calculated results was below 4% at 300–450 K, indicating that this model is useful for the optimum thermal design of high-power HBTs. © 1997 John Wiley & Sons, Inc.* Microwave Opt Technol Lett 16: 38–41, 1997.

Key words: *power HBT; thermal design; Gummel plot; model; thermal measurement; microwave devices*

1. INTRODUCTION

In recent years, AlGaAs/GaAs heterojunction bipolar transistors (HBTs) have demonstrated very high output power and power density at microwave frequencies [1, 2]. However, because of the negative temperature coefficient of base–emitter turn-on voltage and poor thermal conductivity, the output power of HBTs is known to be thermally limited [3]. Therefore, optimum thermal design is necessary to maximize the output power. Many works have been reported to establish the thermal design guide [3–6], and they have used temperature-dependent base or collector current models to calculate the distributions of power density and temperature. But those models are too simple to fit the Gummel plot at various temperatures accurately. Therefore, we propose a new dc model for a Gummel plot, which fits at wide current and temperature ranges with high accuracy. Our model does not need an iterative step in extracting model parameters, and the modeling is very fast.

2. MODEL DESCRIPTION

The proposed model, as well as existing models, basically stems from the well-known diode equation, and is given by Eqs. (1) and (2):

$$I_B = I_{BO}\exp\left[\frac{V_{BE} - R_{\mathrm{EFF},B}I_B + \delta_B(T - T_O)}{\eta_B \kappa T/q}\right] + I_{BO,\mathrm{SCR}}\exp\left[\frac{V_{BE} + \delta_{B,\mathrm{SCR}}(T - T_O)}{\eta_{B,\mathrm{SCR}}\kappa T/q}\right] \quad (1)$$

$$I_C = I_{CO}\exp\left[\frac{V_{BE} - R_{\mathrm{EFF},C}I_C + \delta_C(T - T_O)}{\eta_C \kappa T/q}\right] \quad (2)$$

where I_{BO}, $I_{BO,\mathrm{SCR}}$, and I_{CO} are the saturation currents of the base, base space-charge region recombination, and collector at $T = T_O$, respectively; V_{BE} is the base–emitter voltage; $R_{\mathrm{EFF},B}$ and $R_{\mathrm{EFF},C}$ are the effective parasitic resistance of the base and collector currents, and are given by $R_B + (1 + \beta)R_E$ and $R_B/\beta + (1 + 1/\beta)R_E$, respectively; δ_B, $\delta_{B,\mathrm{SCR}}$, and δ_C are the temperature coefficients of various currents on the base–emitter turn-on voltage, and are affected by the energy gap of the device material [7] and temperature; and η_B, $\eta_{B,\mathrm{SCR}}$, and η_C are the ideality factors of the base, base space-charge region recombination, and collector currents, respectively.

In the case of existing models [3, 4], it is assumed that the parasitic resistance δ and thermal voltage $(\kappa T_O/q)$ are constants. The resulting model can fit a Gummel plot only at a narrow range of current and temperature. To solve this problem, we use temperature- and V_{BE}-dependent effective parasitic resistance, temperature-dependent δ, and $\kappa T/q$:

$$R_{\mathrm{EFF},B\text{ or }C} = a_{B\text{ or }C} + b_{B\text{ or }C}V_{BE} + c_{B\text{ or }C}V_{BE}^2 \quad (3)$$

where

$$a_{B\text{ or }C} = a_{0,B\text{ or }C} + a_{1,B\text{ or }C}T + a_{2,B\text{ or }C}T^2 + a_{3,B\text{ or }C}T^3 + a_{4,B\text{ or }C}T^4 \quad (3a)$$

$$b_{B\text{ or }C} = b_{0,B\text{ or }C} + b_{1,B\text{ or }C}T + b_{2,B\text{ or }C}T^2 + b_{3,B\text{ or }C}T^3 + b_{4,B\text{ or }C}T^4 \quad (3b)$$

$$c_{B \text{ or } C} = c_{0, B \text{ or } C} + c_{1, B \text{ or } C}T + c_{2, B \text{ or } C}T^2 + c_{3, B \text{ or } C}T^3 + c_{4, B \text{ or } C}T^4 \quad (3c)$$

$$\delta_{B, \text{ or } B, \text{SCR}, \text{ or } C} = \delta_{0, B, \text{ or } B, \text{SCR}, \text{ or } C} + \delta_{1, B, \text{ or } B, \text{SCR}, \text{ or } C}T + \delta_{2, B, \text{ or } B, \text{SCR}, \text{ or } C}T^2. \quad (4)$$

$R_{\text{EFF}, B}$ and $R_{\text{EFF}, C}$ are expressed as second-order polynomials of V_{BE}. The coefficients are temperature-dependent, and are fitted using fourth-order polynomials. δ_B, $\delta_{B,\text{SCR}}$, and δ_C are fitted using second-order polynomials of temperature function. The thermal voltage is given by $\kappa T/q$ instead of $\kappa T_O/q$ to describe the Gummel plot more accurately.

3. RESULTS AND DISCUSSIONS

In order to test the model accuracy, Gummel plots of AlGaAs/GaAs HBT with emitter size of 3×30 μm^2 were measured at ambient temperatures between 300 and 450 K at intervals of 25 K. Figure 1 shows the temperature dependence of the base and collector currents. In order to minimize the junction temperature rise above the externally ap-

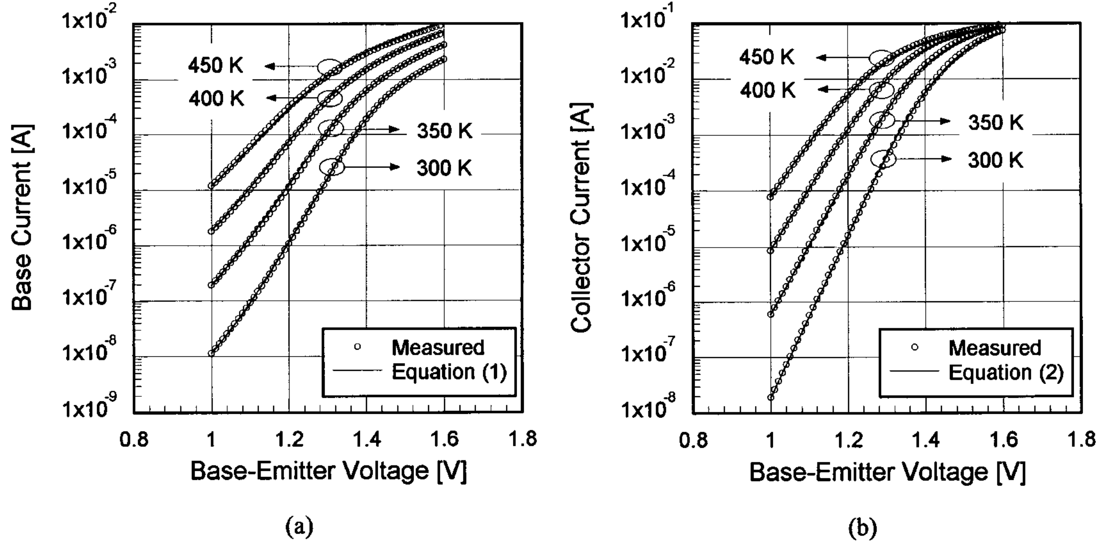

Figure 1 Measured and calculated Gummel plot at $T = 300-450$ K: (a) base current, (b) collector current

Calculate η_B at the steepest slope and 300 °K

$$\eta_B = \frac{V_{BE2} - V_{BE1}}{\log(I_{B2}) - \log(I_{B1})} \cdot \frac{\log_{10} e}{\kappa T / q}$$

Calculate I_{BO} at the steepest slope and 300 °K

$$I_{BO} = \frac{I_B}{\exp\left(\frac{V_{BE}}{\eta_B \kappa T / q}\right)}$$

Calculate δ_B at the steepest slope and various temperatures and fit using Eqn. (4)

$$\delta_B = \frac{-V_{BE} + \eta_B(\kappa T / q)\ln(I_B / I_{BO})}{T - T_O}$$

Extract $R_{EFF,B}$, fit using Eqn. (3) at each temperature and fit a_B, b_B, c_B using Eqns. (3-a), (3-b), and (3-c)

$$R_{EFF,B} = \frac{V_{BE} - \eta_B(\kappa T / q)\ln(I_B / I_{BO}) + \delta_B(T - T_O)}{I_B}$$

Calculate I_B which does not contain $I_{B,SCR}$ using Eqn. (1) and calculate $I_{B,SCR}$ from measurement and calculated data

Calculate $\eta_{B,SCR}$ at the lowest current level and 300 °K

$$\eta_{B,SCR} = \frac{V_{BE2} - V_{BE1}}{\log(I_{B,SCR,2}) - \log(I_{B,SCR,1})} \cdot \frac{\log_{10} e}{\kappa T / q}$$

Calculate $I_{BO,SCR}$ at the lowest current level and 300 °K

$$I_{BO,SCR} = \frac{I_{B,SCR}}{\exp\left(\frac{V_{BE}}{\eta_{B,SCR} \kappa T / q}\right)}$$

Calculate $\delta_{B,SCR}$ at the lowest current level and various temperatures and fit using Eqn. (4)

$$\delta_{B,SCR} = \frac{-V_{BE} + \eta_{B,SCR}(\kappa T / q)\ln(I_{B,SCR} / I_{BO,SCR})}{T - T_O}$$

End

Figure 2 Flowchart of the procedure to extract the model parameters

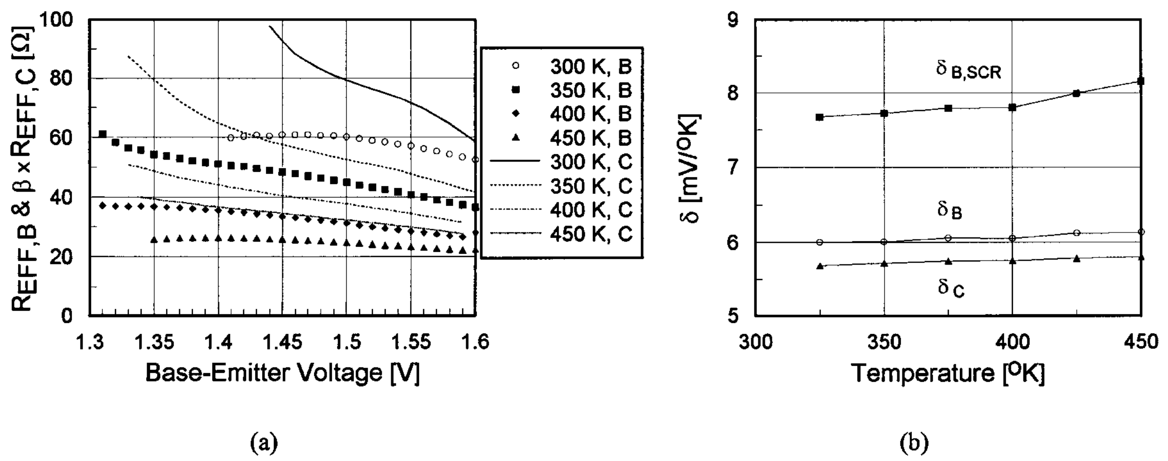

Figure 3 Extracted parameters from measured Gummel plot: (a) effective parasitic resistances, (b) temperature coefficients of the base–emitter turn-on voltage

plied ambient temperature, the base–collector voltage was maintained at 0 V. The procedure to obtain the model parameters for the base current is shown in Figure 2. In order to extract η_B, I_{BO}, δ_B, we take the values at the steepest slope, where one can neglect the space-charge region recombination and parasitic resistance effects. Although there are many model parameters for the effective parasitic resistance, the extraction method is easy and fast because the algorithm for the coefficients is well known [8]. Because there is no iterative procedure to obtain the model parameters, it is very simple and fast to fit the thermal measurement data. The procedure for the collector current is very similar to that for the base current, except for the space-charge region recombination current. The parameters used in the calculations are: $I_{BO} = 4.3 \times 10^{-21}$ A, $I_{BO,\mathrm{SCR}} = 1.3 \times 10^{-14}$ A, $I_{CO} = 4.7 \times 10^{-23}$ A, $\eta_B = 1.4$, $\eta_{B,\mathrm{SCR}} = 2.9$, $\eta_C = 1.15$, and $T_O = 300$ K. The extracted $R_{\mathrm{EFF},B}$ and $\beta \times R_{\mathrm{EFF},C}$ are plotted in Figure 3(a). Because the current gain β decreases as temperature increases, $R_{\mathrm{EFF},B}$ and $\beta \times R_{\mathrm{EFF},C}$ also decrease. $R_{\mathrm{EFF},B}$ is different from $\beta \times R_{\mathrm{EFF},C}$, although they have the same meaning as $R_B + (1 + \beta)R_E$ because the base current is affected by the space-charge region recombination current $I_{B,\mathrm{SCR}}$ up to a medium current level. Therefore, it is very difficult to extract η_B which is not affected by $I_{B,\mathrm{SCR}}$. $R_{\mathrm{EFF},B}$ is somewhat lower than $\beta \times R_{\mathrm{EFF},C}$. Figure 3(b) shows the temperature dependence of δ_B, $\delta_{B,\mathrm{SCR}}$, and δ_C. Saturation currents increase as temperature increases, and we fit the effect using δs. Figure 1 also shows the fitted data using our model. One can see that excellent agreement is obtained between measurement and fitted results over all current and temperature ranges. Figure 4 shows the error between measurement and fitted data at various V_{BE} and temperatures. The maximum errors of the base and collector currents are below 10 and 13%, respectively, and the average error is below 3.5% over all V_{BE} and temperature ranges measured, indicating that our model can be useful for the thermal design of high-power HBTs.

4. CONCLUSIONS

We have established a dc model applicable for a Gummel plot at various temperatures. Our model fits the Gummel plot with good accuracy at wide current and temperature ranges,

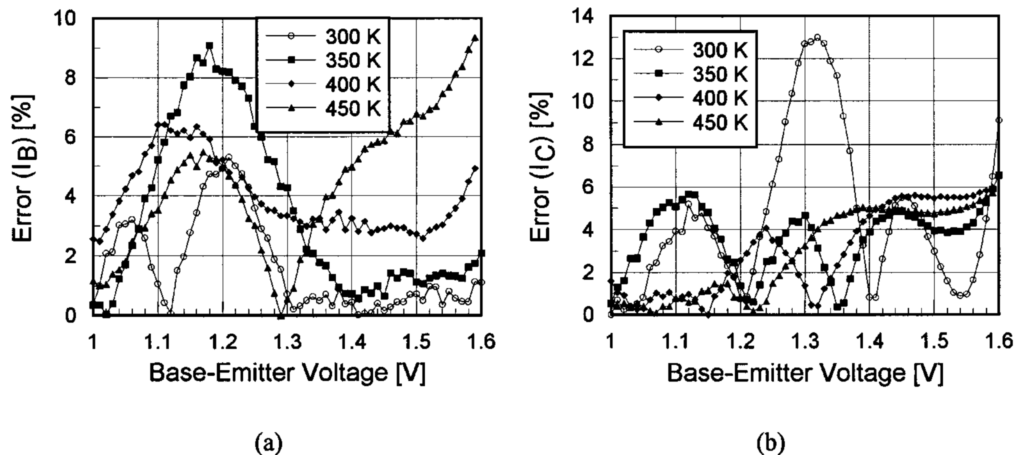

Figure 4 Errors between measured and calculated Gummel plot at $T = 300$–450 K: (a) base current, (b) collector current

and the procedure is straightforward. This model is suitable for the thermal design of high-power HBTs and HBT large-signal models, which includes the self-heating effect.

ACKNOWLEDGMENT

This work was supported in part by the Agency for Defense Development of Korea.

REFERENCES

1. P. K. Ikalainen, S. K. Fan, and M. A. Khatibzadeh, "20 W Linear, High Efficiency Internally Matched HBT at 7.5 GHz," *IEEE MTT-S Dig*., Vol. 2, 1994, pp. 679–681.
2. B. Bayraktaroglu, J. Barrette, L. Kehias, C. I. Huang, R. Fitch, R. Neidhard, and R. Scherer, "Very High-Power-Density CW Operation of GaAs/AlGaAs Microwave Heterojunction Bipolar Transistors," *IEEE Electron Device Lett*., Vol. 14, Oct. 1993, pp. 493–495.
3. L. L. Liou and B. Bayraktaroglu, "Thermal Stability Analysis of AlGaAs/GaAs Heterojunction Bipolar Transistors with Multiple Emitter Fingers," *IEEE Trans. Electron Devices*, Vol. 41, May 1994, pp. 629–636.
4. W. Liu, S. Nelson, D. G. Hill, and A. Khatibzadeh, "Current Gain Collapse in Microwave Multifinger Heterojunction Bipolar Transistors Operated at Very High Power Densities," *IEEE Trans. Electron Devices*, Vol. 40, Nov. 1993, pp. 1917–1927.
5. W. Zhou, S. Sheu, J. J. Liou, and C. I. Huang, "Analysis of Non-Uniform Current and Temperature Distributions in the Emitter Finger of AlGaAs/GaAs Heterojunction Bipolar Transistors," *Solid-State Electron*., Vol. 39, No. 12, 1996, pp. 1709–1721.
6. G. B. Gao, M. Z. Wang, X. Gui, and H. Morkoç, "Thermal Design Studies of High-Power Heterojunction Bipolar Transistors," *IEEE Trans. Electron Devices*, Vol. 36, May 1989, pp. 854–863.
7. G. B. Gao, M. S. Ünlü, H. Morkoç, and D. L. Blackburn, "Emitter Ballasting Resistor Design for, and Current Handling Capability of AlGaAs/GaAs Power Heterojunction Bipolar Transistors," *IEEE Trans. Electron Devices*, Vol. 38, Feb. 1991, pp. 185–196.
8. W. H. Press, S. A. Teukolsky, W. T. Vetterling, and B. P. Flannery, *Numerical Recipes in C*, Cambridge University Press, Cambridge, England, 1992.

© 1997 John Wiley & Sons, Inc.
CCC 0895-2477/97

INPUT IMPEDANCE OF A PROBE-FED CYLINDRICAL ANNULAR-RING MICROSTRIP ANTENNA

Chih-Yu Huang[1] and Wen-Shyang Chen[2]
[1]Department of Electronic Engineering
Yung Ta Junior College of Technology and Commerce
Pingtung, Taiwan, R.O.C.
[2]Department of Electronic Engineering
Chengshiu Junior College of Technology and Commerce
Kaohsiung, Taiwan, R.O.C.

Received 20 March 1997; revised 22 April 1997

ABSTRACT: *An analysis using a generalized transmission line model (GTLM) for a probe-fed cylindrical annular-ring microstrip antenna is presented. The equivalent circuit elements for the microstrip antenna modeled as a transmission line loaded with wall admittances are derived, and the expression for the input impedance is given. Numerical results for the antenna excited at the TM_{12} mode are also calculated and compared with the measured ones, and the effects of different feed positions and cylinder radii on the input impedance are analyzed. Good agreement of the GTLM solutions with the experimental results is observed.* © *1997 John Wiley & Sons, Inc.* Microwave Opt Technol Lett 16: 41–44, 1997.

Key words: *annular ring antenna; input impedance; generalized transmission line model; microstrip antenna*

1. INTRODUCTION

Studies of microstrip antennas are an innovative activity in the antenna field for their low profile, light weight, and conformability. More and more applications are booming; for instance, we may have conformal antennas on the wall of a building instead of bulky parabolic antennas on the roofs of automobiles, inside a cellular phone, and on cylindrical surfaces of missiles, satellites, and aircraft. A number of investigations of the design and analysis have been made, and the characteristics of the microstrip antennas on a planar grounded substrate have been well known. However, the performance of microstrip antennas mounted on a curved surface is still not fully understood.

A transmission line model (TLM) for the analysis of microstrip antennas is simple; the accuracy of the TLM analysis can be made comparable to that of other more complicated methods. However, the TLM method is only applicable for planar rectangular microstrip antennas. The generalized transmission line model (GTLM) was proposed in [1], which is applicable to any shape as long as the separation of variables is possible for the wave equation expressed in that particular coordinate system, such as planar–circular, planar–annular-ring [2], cylindrical–rectangular, cylindrical–circular microstrip antenna [3], and spherical–circular microstrip antenna. In this paper, we study the cylindrical annular-ring microstrip antenna using the GTLM theory. In this model, the radiating apertures are around the patch edges. Therefore, the transmission lines can be taken in the direction normal to the radiating apertures. The mutual admittance between the radiating edges is also included in the GTLM solution, and the input impedance of a microstrip antenna is formulated. Typical results for the input impedance operating at TM_{12} mode are presented and discussed. The effects of different feed positions and cylinder radii on the input impedance are analyzed.

2. THEORY

Figure 1 shows the geometry of an annular-ring microstrip antenna mounted on a ground cylinder of infinite length with radius a. The annular-ring patch has an inner radius b_1 and outer radius b_2, and the substrate has a thickness of h and a relative permittivity ε_r. The outer medium ($\rho > a + h$) is free space with permittivity ε_0 and permeability μ_0. To solve the problem, we adopt new coordinates ($\hat{\rho}, \hat{l}, \hat{\beta}$) [3] as shown in Figure 1. The relations between the components of a vector in the new coordinates and cylindrical coordinates ($\hat{\rho}, \hat{\phi}, \hat{z}$) can be written in a matrix form:

$$\begin{bmatrix} A_\rho \\ A_l \\ A_\beta \end{bmatrix} = \begin{bmatrix} 1 & 0 & 0 \\ 0 & \cos\beta & \sin\beta \\ 0 & -\sin\beta & \cos\beta \end{bmatrix} \begin{bmatrix} A_\rho \\ A_\phi \\ A_z \end{bmatrix}. \tag{1}$$

In this case, the feed positions of the annular-ring patch can be expressed to be at $(l', \beta') = (d, \beta_0)$. By considering the condition that the substrate thickness is much less than one wavelength and $h \ll a$, the electric field under the patch has only a radial component E_ρ, which is independent of ρ.